SHORT TITLE

Multiplex knockout using a single gRNA

ARTICLE TITLE

Multiplex knockout of trichome-regulating MYB duplicates in hybrid poplar using a single gRNA

ONE SENTENCE SUMMARY

Targeting conserved sequences with a single gRNA allowed efficient mutagenesis of a multigene family and the recovery of trichomeless and triterpene-free poplar mutants.

AUTHORS

W. Patrick Bewg[1,2,3], Scott A. Harding[1,2,3], Nancy L. Engle[4], Brajesh N. Vaidya[5,a], Ran Zhou[1,2,3], Jacob Reeves[6,b], Thomas W. Horn[6], Nirmal Joshee[5], Jerry W. Jenkins[7,8], Shengqiang Shu[8], Kerrie W. Barry[8], Yuko Yoshinaga[8], Jane Grimwood[7,8], Robert J. Schmitz[2], Jeremy Schmutz[7,8], Timothy J. Tschaplinski[4], and Chung-Jui Tsai[1,2,3*]

[1] *School of Forestry and Natural Resources, University of Georgia, Athens, Georgia, 30602, USA*

[2] *Department of Genetics, University of Georgia, Athens, Georgia, 30602, USA*

[3] *Department of Plant Biology, University of Georgia, Athens, Georgia, 30602, USA*

[4] *Oak Ridge National Laboratory, Oak Ridge, Tennessee, 37830, USA*

[5] *Fort Valley State University, Fort Valley, Georgia, 31030, USA*

[6] *Department of Computer Science, University of Georgia, Athens, Georgia, 30602, USA*

[7] *HudsonAlpha Institute for Biotechnology, Huntsville, Alabama, 35806, USA*

[8] *U.S. Department of Energy Joint Genome Institute, Berkeley, California, 94720, USA*

**Senior author and author for correspondence: cjtsai@uga.edu (C.-J.T.)*

[a] *Present address: GreenVenus, LLC, Wimauma, Florida 33598, USA*

[b] *Present address: SoundHound Inc., Boulder, Colorado 80302, USA*

The author responsible for distribution of materials integral to the findings presented in this article in accordance with the policy described in the Instructions for Authors is Chung-Jui Tsai (cjtsai@uga.edu).

AUTHOR CONTRIBUTIONS

C.-J.T. and W.P.B. conceived the study and designed the experiments; W.P.B. performed all experiments and analyzed data; S.A.H. provided guidance on physiological and metabolic analyses; J.R., T.W.H, and R.Z. provided bioinformatic support; B.N.V. and N.J. performed SEM analysis; J.J., K.B., R.J.S., Y.Y., S.S., J.G. and J.S. contributed the *Populus tremula* x *P. alba* INRA 717-1B4 draft genome; N.L.E. and T.J.T. performed wax compositional analysis; W.P.B. and C.-J.T. wrote the manuscript, with input from S.A.H.

FUNDING

The work was funded in part by The Center for Bioenergy Innovation, a U.S. Department of Energy Research Center supported by the Office of Biological and Environmental Research in the DOE Office of Science, the Division of Integrative Organismal Systems (grant nos. IOS-1546867) of the National Science Foundation, the Community Science Program of the Joint Genome Institute, a DOE Office of Science User Facility. The work conducted by the U.S. Department of Energy Joint Genome Institute is supported by the Office of Science of the U.S. Department of Energy under Contract No DE-AC02-05CH11231.

Keywords: multiplex editing, gene duplication, triterpenes, glabrous, genomic dropout

ABSTRACT

As the focus for CRISPR edited plants moves from proof-of-concept to real world applications, precise gene manipulation will increasingly require concurrent multiplex editing for polygenic traits. A common approach for editing across multiple sites is to design one gRNA per target; however, this complicates construct assembly and increases the possibility of off-target mutations. In this study, we utilized one gRNA to target *MYB186*, a known positive trichome regulator, as well as its paralogs *MYB138* and *MYB38* at a consensus site for mutagenesis in *Populus tremula* × *P. alba* INRA 717-1B4. Unexpected duplications of *MYB186* and *MYB138* resulted in a total of eight alleles for the three targeted genes in the hybrid poplar. Deep sequencing and PCR analyses confirmed editing across all eight targets in nearly all of the resultant glabrous mutants, ranging from small indels to large genomic dropouts, with no off-target activity detected at four potential sites. This highlights the effectiveness of a single gRNA targeting conserved exonic regions for multiplex editing. Additionally, cuticular wax and whole leaf analyses showed a complete absence of triterpenes in the trichomeless mutants, hinting at a previously undescribed role for the non-glandular trichomes of poplar.

97 **INTRODUCTION**

98

99 CRISPR (clustered regularly interspaced short palindromic repeats) technology has been adopted for
100 plant genome editing in an increasing number of species for both basic and applied research (Bewg et
101 al., 2018; Chen et al., 2019; Nasti and Voytas, 2021). The power of CRISPR is due in part to its simplicity
102 with just two core components (Jinek et al., 2012): a nuclear-localized endonuclease, such as CRISPR-
103 associated Cas9 that works universally across all domains of life and a synthetic guide RNA (gRNA) that is
104 customizable and scalable for sequence-specific targeting. With its proven precision and efficiency (Li et
105 al., 2013; Nekrasov et al., 2013; Shan et al., 2013; Endo et al., 2016) and given the polygenic nature of
106 many agronomic traits, there is growing interest in targeting multiple loci for simultaneous CRISPR
107 editing to aid gene function investigation and/or trait engineering (Armario Najera et al., 2019).

108

109 Multiplex editing usually involves coexpression of multiple guide RNAs (gRNAs). For the classic
110 CRISPR/Cas9 system, this has been demonstrated using individual gRNA cassettes each driven by a
111 separate RNA polymerase III (Pol III) promoter (Xing et al., 2014; Lowder et al., 2015; Ma et al., 2015).
112 Alternatively, multiple gRNAs can be expressed in tandem with tRNAs as a single polycistronic transcript
113 and processed into individual gRNAs using endogenous tRNA processing machinery (Xie et al., 2015).
114 Polycistronic gRNA transcripts have also been engineered with built-in RNA cleavage sites for processing
115 by ribozymes or the CRISPR-associated endoribonuclease Csy4 (Qi et al., 2012; Gao and Zhao, 2014;
116 Tang et al., 2016; Čermák et al., 2017; Tang et al., 2019). In several cases, functional gRNAs were
117 generated from a single transcriptional unit of *Cas9* fused with an artificial gRNA array without specific
118 flanking sequences (Mikami et al., 2017; Wang et al., 2018). It has been reported that up to eight gRNAs
119 have been successfully deployed for multiplex editing (Ma et al., 2015; Xie et al., 2015; Čermák et al.,
120 2017).

121

122 An understudied approach is the use of single gRNAs to target homologous sequences at discrete loci.
123 The capability was showcased by effective inactivation of all 62 copies of porcine endogenous
124 retroviruses in an immortalized pig cell line using two gRNAs to target a highly conserved region of the
125 polymerase (*pol*) gene (Yang et al., 2015). Besides parasitic elements, a single consensus gRNA has also
126 been used to edit paralogs derived from various gene duplication events in soybean and sorghum
127 (Jacobs et al., 2015; Li et al., 2018) or homoeologs in polyploid wheat and oilseed rape (Braatz et al.,
128 2017; Zhang et al., 2017). Multiplex targeting of duplicated genes is especially important for

129 investigation of functional redundancy in plant genomes that are shaped by whole-genome, segmental,
130 tandem, and/or transposon-mediated duplications (Flagel and Wendel, 2009; Panchy et al., 2016).
131 Depending on the duplication age and subsequent selection constraints, sequence similarity can be very
132 high among duplicates, enabling identification of consensus target sites for multiplex editing by a single
133 gRNA. This approach greatly simplifies construct design and assembly, reduces off-target potential that
134 increases with the number of gRNAs (McCarty et al., 2020), and can be bundled with other multi-gRNA
135 editing strategies discussed above for higher-order multiplex targeting of distinct gene families.
136
137 The present study explored the utility of a single gRNA for multiplex editing in an outcrossing woody
138 perennial, *Populus tremula* × *P. alba* INRA 717-1B4 (hereon referred to as 717). As an interspecific
139 hybrid, the 717 genome is highly heterozygous which presents additional challenges to gRNA design and
140 edit outcome determination (Xue et al., 2015). Using trichomes as visual reporter, we targeted a known
141 positive regulator of trichome development, *PtaMYB186* (Plett et al., 2010), and its close paralogs
142 *PtaMYB138* and *PtaMYB38* for knockout (KO). We show that a single gRNA with SNP-aware design is
143 effective for multiplex KO of paralogous genes and robust against copy number variations in a hybrid
144 genome with an unexpected tandem duplication in one of its sub-genomes. We employed multiple
145 approaches to address the analytical challenge of discriminating among highly similar target sites to
146 discern mutations that ranged from small indels to large genomic dropouts. Finally, analysis of the
147 resultant trichomeless mutants revealed a complete absence of triterpenes, and implicated a role for
148 poplar trichomes in triterpene accrual.
149
150
151 **RESULTS**
152
153 **Multiplex CRISPR/Cas9 editing of trichome-regulating MYBs**
154 The known positive regulator of trichome initiation *PtaMYB186* (Plett et al., 2010) corresponds to gene
155 model Potri.008G089200 in the *P. trichocarpa* v3.1 genome. It belongs to clade 15 of the R2R3-MYB
156 protein family tree (Wilkins et al., 2009), which is expanded in poplar and contains three additional
157 members, *MYB138*, *MYB38* and *MYB83*, with as yet unclear functions. The four clade 15 members are
158 derived from multiple duplication events, based on whole paranome K_S (synonymous distance)
159 distribution and gene collinearity analyses using the wgd program (Zwaenepoel and Van de Peer, 2018).
160 These include an ancient (gamma) whole genome duplication (*MYB186* and *MYB83*, $K_S = 3.76$), a Salicoid

161 duplication (*MYB186*/*MYB138* and *MYB38*, K_S = 0.21-0.22), and a tandem duplication (*MYB186* and
162 *MYB138*, K_S = 0.0001) (Figure 1). MYB186, MYB138 and MYB38 share higher levels (88-96%) of amino
163 acid sequence similarity than with MYB83 (55-57%). To ascertain these MYB involvement in trichome
164 development, we mined RNA-seq data from different stages of 717 leaf development. Transcript levels
165 of *MYB186*, *MYB138* and *MYB38* were highest in newly emerged leaves (Leaf Plastochron Index LPI-1)
166 when trichome initiation occurs (Plett et al., 2010), but quickly declined thereafter in expanding (LPI-5)
167 and mature (LPI-15) leaves (Figure 1). In contrast, *MYB83* transcripts were detected throughout leaf
168 maturation (Figure 1), weakening support for its potential involvement in trichome development.
169
170 We designed a single gRNA to target a conserved region in exon two of *MYB186*, *MYB138* and *MYB38*
171 (Figure 2A) based on the *P. trichocarpa* v3.1 reference genome and cross-checked using the 717 variant
172 database (Xue et al., 2015; Zhou et al., 2015) to assure the gRNA target sites were SNP-free in 717. Two
173 CRISPR/Cas9 constructs were generated (see Methods); the first erroneously omitted a guanine
174 between the gRNA and the scaffold sequences (referred to as ΔG, Figure 2B), which was corrected in the
175 second construct (Figure 2A). Both constructs were used for 717 transformation in order to learn
176 whether ΔG would affect CRISPR/Cas9 editing. In total, 28 independent events generated from the ΔG
177 construct were all phenotypically indistinguishable from the wild type (WT) and Cas9-only controls
178 (Figure 2C-J). In contrast, 37 independent events generated from the correct knock out (KO) construct
179 were glabrous (Figure 2N-R), and one glabrous-like event (KO-27) had a greatly reduced trichome
180 density across all shoot tissues (leaf, petiole and stem) independent of age (Figure 2K-M). SEM imaging
181 revealed no trichome initiation or development on the abaxial leaf surface of the glabrous mutants
182 (Figure 2Q). Epidermal cell morphology of young leaves from tissue cultured plants did not differ
183 between control and mutant genotypes on either their abaxial (Figure 2F, N) or adaxial surfaces (Figure
184 2J, R). These results are consistent with roles for MYB186 (Plett et al., 2010) and its paralogs MYB138
185 and MYB38 in trichome initiation and development.
186
187 **Mutation spectrum of duplicated 717 *MYB* alleles**
188 A random selection of 30 glabrous events, 28 ΔG events, two Cas9-only events and four WT plants were
189 subject to amplicon deep-sequencing using consensus primers for *MYB186*, *MYB138* and *MYB38*. Initial
190 analysis by AGEseq (Xue and Tsai, 2015) showed numerous chimeric edits (mix of edited and unedited
191 sequences at a given site) not observed in other CRISPR/Cas9-edited 717 transgenics in our experience
192 (Zhou et al., 2015; Bewg et al., 2018; Tsai et al., 2020). *De novo* assembly of amplicon reads from control

193 samples revealed seven distinct sequences, more than the expected six alleles of the three target genes.
194 Blast search against the preliminary 717 genome assemblies by the Joint Genome Institute uncovered an
195 unexpected copy number variation in 717 relative to the *P. trichocarpa* reference genome. The region
196 containing paralogous *MYB186* and *MYB138* on Chromosome (Chr) 8 is found as a tandem duplicate in
197 one of the 717 subgenomes (Figure 3A). This results in three alleles each for *MYB186* and *MYB138* (two
198 on the main subgenome [Chr8m] and one on the alternative subgenome [Chr8a]) and two alleles for
199 *MYB38* on Chr10 (Chr10m and Chr10a, Figure 3A). Two of the eight alleles were identical in the (original)
200 amplicon region, explaining the seven distinct sequences we recovered from *de novo* assembly. Based
201 on the 717 assemblies, we redesigned primers to ensure the amplicons span allele-specific SNP(s) to aid
202 mutation pattern determination of the eight alleles.
203
204 Amplicon-sequencing showed no editing in the 28 ΔG events, except one (ΔG-24) with a 9 bp deletion at
205 one of the eight target sites (Supplemental Dataset S1). This translates into a mutation rate of 0.45%
206 (one out of 224 potential target sites), which suggests a negative effect of the ΔG on CRISPR/Cas9
207 function (hereafter, the ΔG plants were treated as transformation controls). In contrast, we confirmed
208 successful editing across the eight alleles in all glabrous mutants except KO-27 (Figure 3B-C,
209 Supplemental Dataset S1). This event showed six edited and two WT (unedited) alleles, consistent with
210 trichome detection in this line (Figure 2K-M). In aggregate, small insertions and deletions (indels) were
211 the predominant edits at all sites (Figure 3B-D), with frameshift deletions of 1 bp (-1), 2 bp (-2) and 4 bp
212 (-4) accounting for over three quarters of the indel mutations (Figure 3D). In-frame deletions (-3 or -6)
213 accounted for 10% of indels and were detected in 14 events, including KO-27 (Figure 3B-DThese in-
214 frame mutations are unlikely functional because the gRNA target site is located within the third α-helix
215 of the R2 domain critical for MYB-DNA interaction (Wang et al., 2020), and because 13 of the events
216 with in-frame mutations are glabrous. We therefore conclude that all small indels we detected are null
217 mutations.
218
219 **Large genomic dropouts between tandem genes**
220 The vast majority (80%) of the sequenced mutants also harbored potentially large deletions as
221 evidenced by the dearth of mapped amplicon reads at the target sites, referred to as no-amplification
222 (NA) alleles (Figure 3B-D, Supplemental Dataset S1). The NA frequencies differed by chromosome
223 position and were positively correlated with copy number, being highest at the Chr8m sites (four
224 tandem copies), followed by the Chr8a sites (two tandem copies) and least at the single-copy Chr10 sites

225 (Figure 3A-B). The NA alleles on Chr8 often spanned consecutive copies, suggesting large dropouts
226 between two gRNA cleavage sites. To support this idea, we examined a subset of mutant lines using
227 allele-specific primers for PCR amplification of the target genes. As expected, NA alleles yielded no PCR
228 products, whereas alleles previously detected by amplicon sequencing produced observable PCR
229 products (Supplemental Figure S1). We next used consensus primers for PCR amplification of all six Chr8
230 (*MYB186* and *MYB138*) alleles, approximately 850 – 950 bp, from three control plants and four KO lines
231 each with 4-5 NA alleles on Chr8. These KO lines had reduced PCR band intensity when compared with
232 controls (Figure 4A-B). Sanger sequencing of the PCR products resulted in clean chromatograms with
233 clear nucleotide peaks throughout the sequenced length for KO-5 and KO-69 (Figure 4C), two mutant
234 lines with only one detectable Chr8 allele (Figure 4B). In contrast, the chromatograms for KO-63, KO-70
235 (both containing two detectable Chr8 alleles) and WT samples were noisy as would be expected for
236 mixed template (Figure 4B-C). The Sanger sequencing data of KO-5 and KO-69 not only confirmed the
237 indel pattern (-2 in both cases) detected by amplicon sequencing, but also supported the occurrence of
238 gene fusion between two gRNA cleavage sites, based on SNP patterns upstream and downstream of the
239 gRNA target (Figure 4B-C). KO-5 harbors a fusion junction between *MYB186m1* and *MYB138m1* with a
240 ~29 Kb genomic dropout, whereas KO-69 contains a fusion of *MYB138m1* and *MYB138m2* with a ~62 Kb
241 genomic dropout (Figure 4B-C, Supplemental Figure S2). Both events likely contain additional large
242 deletions or genomic fusions, as allele(s) downstream (KO-5) or upstream (KO-69) of the respective
243 fusion point could not be PCR amplified (Figure 4B). Regardless, our findings show that a single gRNA is
244 highly effective for multiplex KO of tandem duplicates via either small indels or large deletions.
245
246 **Assessment of off-target activity in mutants**
247 A combination of computational prediction and experimental verification was used to assess off-target
248 effects. Potential off-target sites of the gRNA were predicted by CCTop (Stemmer et al., 2015) using the
249 *P. trichocarpa* v3.1 reference genome as well as the two SNP-substituted Pta717 v2 (*P. alba* and *P.*
250 *tremula*) subgenomes (Xue et al., 2015). The same four exonic locations were ranked among the top
251 potential off-target sites (excluding intergenic or unassembled scaffold sequences) across the three
252 genomes, each having three mismatches with the gRNA sequence. We designed three sets of primers to
253 examine potential editing at the four off-target sites; OT1 (Potri.004G115600 and Potri.004G118000),
254 OT2 (Potri.004G138000), and OT3 (Potri.014G024400). Amplicon sequencing of 20 trichomeless mutants
255 found no off-target activity across these four sites (Supplemental Dataset S2).
256

257 **Absence of triterpenes in trichomeless leaves**

258 Trichomes as epidermal outgrowths are covered with waxy cuticles like other epidermis cells (Hegebarth
259 et al., 2016). The striking glabrous phenotype of the mutants prompted us to compare leaf wax
260 composition between control and trichomeless plants. Total wax load of mature leaves (extractable wax
261 from leaf surface) did not change significantly between genotypes (Figure 5A). Alkanes were the most
262 abundant class of leaf cuticular waxes detected in 717 and differed little between control and
263 trichomeless plants (Figure 5B). In contrast, levels of triterpenes, fatty alcohols and β-sitosterol were
264 significantly reduced in the mutants (Figure 5B-D). Specifically, the wax of mutant leaves was devoid of
265 any triterpenes, including α-amyrin, β-amyrin, β-amyrone and lupenone (Figure 5E). Two primary
266 alcohols, 1-octacosanol (C28) and 1-hexacosanol (C26), were depleted in the mutants by >50% (Figure
267 5C), and β-sitosterol, by 42% (Figure 5D). To further investigate the absence of triterpenes in the mutant
268 wax, whole leaf tissues were also profiled for compounds that were significantly reduced in cuticular
269 wax. Again, triterpenes were not detected in the leaves of trichomeless mutants (Figure 5E), whereas 1-
270 octacosanol, 1-hexacosanol and β-sitosterol were detected at levels comparable with controls (Figure
271 5C,D). The data support a previously unsuspected link between triterpene accrual and non-glandular
272 trichomes in poplar.
273
274
275
276 **DISCUSSION**
277
278 The present study demonstrates that a single gRNA targeting conserved genomic sites is highly effective
279 for multiplex editing in poplar. The 30 independent KO lines experienced an average of 5.4 CRISPR/Cas9-
280 mediated cleavages per line based on indel alleles, which is likely an underestimate because many NA
281 alleles may also result from CRISPR/Cas9 cleavages as shown for KO-5 and KO-69 (Figures 3 and 4). The
282 unexpected genomic complexity in the hybrid 717 highlights the importance of ensuring SNP-free
283 targets for gRNA design (Zhou et al., 2015), as well as the challenge of decoding multiplexed edits among
284 highly homologous gene duplicates.
285
286 The negligible editing by the ΔG construct (Supplementary Dataset S1) provides insight into scaffold
287 structure and stability. The ΔG configuration can lead to two hypothetical outcomes: either the guanine
288 is omitted from the scaffold and the gRNA remains intact and capable of base pairing to the target sites

289 for Cas9 cleavage, or the guanine is sequestered for secondary structure folding of the scaffold, resulting
290 in a 3′-truncated gRNA no longer PAM-adjacent at the target sites (Figure 2B). The lack of mutations in
291 ΔG transformants supports the latter scenario and is consistent with transcription and folding of gRNA
292 molecules preceding their base-pairing with genomic targets. Our finding suggests that 3'-truncated
293 gRNA could serve as an alternative approach for generating transgenic controls.
294
295 A number of methods are commonly used for decoding CRISPR-mediated mutation patterns, including
296 restriction digestion, endonuclease-based mismatch detection, gene-/allele-specific PCR sometimes in
297 conjunction with cloning and/or Sanger sequencing (Figure 4), or amplicon deep sequencing (Figure 3).
298 The pros and cons of these methods have been discussed elsewhere (e.g., Germini et al., 2018). Analysis
299 of genome editing across multiple target sites poses additional challenges over mono-targeted
300 experiments, especially when highly homologous target and flanking sequences are encountered. These
301 multiplex scenarios generally exceed the resolution of most methods or may require additional assays
302 (*e.g.*, allele-specific PCR) to determine editing outcomes. In the case exemplified here, deep sequencing
303 of a pooled library of amplicons obtained with consensus primers for all eight target alleles was highly
304 effective for decoding multiplexed edits. The use of consensus primers provides built-in controls for
305 each PCR, allowing for high confidence calling of NA alleles (see Supplemental Dataset S1) which are
306 otherwise difficult to distinguish from failed PCR in individual reactions. As another advantage, the
307 amplicon deep sequencing data can be used for *de novo* assembly which in our case led to the discovery
308 of unexpected copy number variations of MYB186 and MYB138 in the experimental poplar 717
309 genotype. Although technical limitations remain in short-read mapping to highly homologous sites,
310 inclusion of allele-specific SNPs within the amplicon region and adoption of bioinformatic programs with
311 parameter tuning capabilities (*e.g.*, AGEseq) are key to multiplexed mutation pattern determination.
312
313 The glabrous mutants (Figure 2) provide strong support for an essential role of PtaMYB186/138/38 in
314 the initiation of trichome development in 717. Additionally, the low trichome density of KO-27 suggests
315 that MYB38 plays a redundant but minor role in leaf/stem trichome initiation (Figures 2 and 3). Follow-
316 up research, including allele-specific KOs, is needed to dissect the functional redundancy and allele-dose
317 response of clade 15 MYB members more fully. The unedited (WT) *MYB38* alleles in KO-27 appear stable
318 during vegetative propagation as this event has maintained a low trichome density for over two years in
319 both tissue culture and greenhouse environments. This adds to previously reported stability of CRISPR
320 editing outcomes in clonally propagated poplar (Bewg et al., 2018)

321

322 The loss of trichomes did not significantly affect the total epidermal wax load but led to a complete
323 absence of triterpenes both in cuticular wax and whole leaves of the mutants. It is unlikely that
324 MYB186/138/38 have an additional role in triterpene biosynthesis (*i.e.*, lack of triterpenes as a direct KO
325 effect) because of their recent duplication history (Figure 1) and because a recent report implicated
326 phylogenetically distinct MYBs in triterpene regulation (Falginella et al., 2021). We interpret the absence
327 of triterpenes in trichomeless leaves as suggesting a role for non-glandular trichomes in triterpene
328 accrual in poplar. While glandular trichomes are well known for their roles in biosynthesis and storage of
329 terpenes (Lange and Turner, 2013), the presence of terpenes in non-glandular trichomes has only been
330 reported recently (Santos Tozin et al., 2016; Dmitruk et al., 2019). The genetic evidence presented
331 herein provides strong support for a functional link between triterpenes and non-glandular trichomes
332 that warrants further investigation.

333

334 The glabrous phenotype of the null mutants we obtained highlights the potential utility of trichomes as
335 a visual reporter. Assessments of CRISPR/Cas functionality often target the chlorophyll biosynthetic
336 enzyme phytoene desaturase (PDS) (Norris et al., 1995), as mutations result in an albino phenotype
337 (Shan et al., 2013; Ma et al., 2015; Xie et al., 2015). Whilst phenotypically obvious, *PDS* mutations are
338 lethal for the regenerated plant, thus limiting follow-up investigations. Alternatively, the glabrous
339 phenotype achieved by KO of trichome-regulating *MYBs* is non-lethal and no inhibition to plant growth
340 was detected. This allows stacked mutagenesis of these mutants, including reparative transformations
341 to restore trichome initiation. The use of trichomes as a visual reporter for CRISPR/Cas9 mutation or
342 repair of a defective allele has been established in Arabidopsis (Hahn et al., 2017; Hahn et al., 2018)
343 which provides support for further developing this system in poplar.

344

345

346 **MATERIALS AND METHODS**

347

348 **Generation of KO mutants**

349 The ΔG and KO constructs in p201N-Cas9 (Jacobs et al., 2015) were prepared by Gibson assembly. PCR
350 was used to amplify the p201N-Cas9 binary vector following *Swa*I (New England BioLabs) digestion, and
351 the *Medicago truncatula Mt*U6.6 promoter and scaffold fragments from HindIII and EcoRI (New England
352 BioLabs) digested pUC-gRNA shuttle vector (Jacobs et al., 2015), with Q5 High-Fidelity DNA Polymerase

353 (New England BioLabs) and primers (Sigma) listed in Supplemental Table S1. The p201N-Cas9 (Addgene
354 59175) and pUC-gRNA (Addgene 47024) plasmids were both gifts from Wayne Parrott. Two pairs of
355 oligos (Sigma) corresponding to the consensus gRNA target site in exon two of *MYB186*
356 (Potri.008G089200), *MYB138* (Potri.008G089700) and *MYB38* (Potri.010G165700) were assembled with
357 p201N-Cas9. The NEBuilder HiFi DNA Assembly Cloning Kit (New England Biolobs) was used to assemble
358 p201N-Cas9, *Mt*U6.6 promoter and scaffold fragments with a pair of oligos containing the gRNA target
359 sequence (Supplemental Table S1). Following transformation into DH5α *E. coli* (Zymo Research Mix &
360 Go! Competent Cells), PCR-positive colonies were used for plasmid purification before Sanger
361 sequencing (Eurofins) confirmation. Plasmids were then heat-shocked into *Agrobacterium tumefaciens*
362 strain C58/GV3101 (pMP90) (Koncz and Schell, 1986) and confirmed by colony PCR.
363
364 *Populus tremula* x *alba* (IRNA 717-1B4) transformation and regeneration was performed as outlined in
365 Meilan and Ma (2006), except 0.05 mg/L 6-benzylaminopurine was used in shoot elongation media, and
366 200 mg/L L-glutamine was added to all media, with 3 g/L gellan gum (PhytoTechnology Lab) as a gelling
367 agent. Following a 2-day agrobacterial cocultivation, leaf discs were washed in sterile water followed by
368 washing in 200 mg/L cefotaxime and 300 mg/L timentin with shaking for 1.5 hr. Transformants were
369 selected on media supplemented with 100 mg/L kanamycin, 200 mg/L cefotaxime and 300 mg/L
370 timentin for callus induction and shoot regeneration and with kanamycin and timentin for shoot
371 elongation and rooting. All cultures were grown and maintained at 22°C under a 16-hr light/8-hr dark
372 photoperiod with Growlite® FPV24 LED (Barron Lighting Group) at ~150 µmol/m^2/s.
373
374 **RNA-seq analysis**
375 For developmental profiling, LPI-1, LPI-5 and LPI-15 were collected from three greenhouse-grown WT
376 plants (~5 ft in height) for RNA extraction using Direct-zol RNA MiniPrep kit (Zymo Research) with Plant
377 RNA Purification Reagent (Invitrogen). RNA-seq library preparation and Illumina NextSeq 500 sequencing
378 was performed at the Georgia Genomics and Bioinformatics Core. We obtained 10.8-13.3 PE75 reads
379 per sample. After pre-processing to remove adapter and rRNA sequences, reads were mapped to the
380 717 SNP-substituted genome sPta717 v2 (Xue et al., 2015) using STAR v2.5.3a (Dobin and Gingeras,
381 2015). Transcript abundance in FPKM (fragments per kilobase of transcript per million mapped reads)
382 was estimated by featureCounts v1.5.2 (Liao et al., 2014).
383
384 **Amplicon sequencing determination of mutation spectrums**

385 Newly emerged leaves were excised from individual events in tissue culture for genomic DNA extraction
386 (Dellaporta et al., 1983). The DNA pellet was resuspended in water with RNase A (10 µg/mL) for
387 amplicon library preparation using GoTaq G2 Green Master Mix (Promega) and primers (Supplemental
388 Table S1) spanning the gRNA target site (between 264 bp to 280 bp). Samples were then barcoded with
389 Illumina amplicon indexing primers and pooled for Illumina MiSeq nano PE150 sequencing performed at
390 the University of Georgia's Georgia Genomics and Bioinformatics Core. Demultiplexed sequence reads
391 were analyzed by the AGEseq (Analysis of Genome Editing by Sequencing) program (Xue and Tsai, 2015),
392 with mismatch allowance set at 1%, followed by manual curation.
393
394 Because initial amplicon data analysis revealed lower editing efficiencies (<90%) than we typically
395 observed in 717 (Zhou et al., 2015; Bewg et al., 2018) at several target sites, we performed *de novo*
396 assembly of WT amplicon reads using Geneious, and recovered seven distinct alleles. We then searched
397 the JGI draft 717 genome assembly v1.0 with the *P. trichocarpa* Nisqually-1 v3.1 (Phytozome v12)
398 *MYB186*, *MYB138* and *MYB38* gene models and extracted the surrounding 50-150 Kb regions from Chr8
399 and Chr10 for manual annotation against the *P. trichocarpa* Nisqually-1 reference (Figure 3A). The
400 matching *MYB* gene sequences were extracted for error correction using 717 resequencing data (Xue et
401 al., 2015). Curated sequences were used for new (amplicon and allele-/gene-specific) primer design and
402 as references in amplicon data analysis. In the case of WT and transgenic controls with no editing,
403 erroneous read assignments—and hence indel calls—still remained because the amplicon region
404 between some alleles differs only in the number of intronic dinucleotide (GT) repeats (Supplemental
405 Dataset S1). Misassigned reads led to erroneous indel calls of -2, +2 or their multiples outside of the
406 gRNA target site. For this reason, WT and control samples were processed by ustacks from Stacks 2.3
407 (Catchen et al., 2011). Parameters were adjusted to avoid collapsing reads with SNPs and/or Indels from
408 paralogous alleles into the same tag group and gapped alignments were disabled. Tags from the output
409 were then used for allele assignment.
410
411 **Determination of leaf and cuticle wax compositions**
412 Leaf punches (25 mm diameter) were taken from mature leaves of similar size (between LPI-10 and LPI-
413 15) of soil-grown plants in a growth chamber and washed in 4 mL of methylene chloride for 30 sec. The
414 washes were dried under a continuous N_2 stream before resuspension in 400 µL chloroform. A 200 µL
415 aliquot was subsequently dried under vacuum and the residues shipped to the Oak Ridge National
416 Laboratory for analysis. Sorbitol (1 mg/mL) was added to the residues as an internal standard and re-

417 dried under N_2. For whole leaf analysis, liquid nitrogen-ground and freeze-dried powders from LPI-5 (25
418 mg) of control and KO plants were extracted by 80% ethanol to which sorbitol (1 mg/mL) was added and
419 dried under N_2. The samples were derivatized prior to analysis on an Agilent Technologies 7890A GC
420 coupled to a 5975C inert XL MS fitted with an Rtx-5MS capillary column with a 5m Integra-Guard column
421 (Restek) as described in Holwerda et al. (2014). Compound identification was based on mass spectral
422 fragmentation patterns against the NIST08 database and an in-house library built with authentic
423 standards.
424
425 **Tissue Imaging and SEM analysis**
426 Images of poplar were taken with either a Google Pixel 3a running Android v11, or a Leica M165 FC
427 dissection microscope attached to a Leica DFC500 camera running Leica Application Suite software
428 v3.8.0. Scanning electron microscopic (SEM) observations were obtained using Hitachi 3400 NII (Hitachi
429 High Technologies America) microscope following optimized protocols at the Center for Ultrastructural
430 Research at the Fort Valley State University. LPI-1 from growth chamber plants or young leaves of tissue
431 culture plants were processed for primary fixation at 25°C in 2 % glutaraldehyde (Electron Microscopy
432 Sciences, EMS) prepared with Sorensen's Phosphate buffer, pH 7.2 (EMS) for one hour and then washed
433 three times for 15 min each with the same buffer before secondary fixation in 1% osmium tetroxide
434 (EMS) prepared in Sorensen's Phosphate buffer, pH 7.2 for 1 hour at 25°C. After three washes with dH_2O
435 for 15 min each, fixed tissues were dehydrated with ethanol series passing through 25%, 50%, 75%, and
436 95% for 15 min each, followed by three changes of 100% ethanol for 15 min each. Critical point drying of
437 fixed samples was conducted using a critical point dryer (Leica) and then samples were placed on Hitachi
438 M4 aluminum specimen mounts (Ted Pella) using double sided carbon adhesive tabs (EMS) for coating.
439 Gold coating of 50 Å thickness was done for 60 sec using sputter coater (Denton Desk V) under a vacuum
440 pressure of 0.05 torr. Image acquisition in various magnification was done at accelerating voltage of 5
441 KV.
442
443 **ACCESSION NUMBERS**
444 The RNA-seq data has been deposited to the National Center for Biotechnology Information's Sequence
445 Read Archive under accession No. PRJNA753499.
446
447 **ACKNOWLEDGEMENTS**

The authors thank Gilles Pilate of the Institut National de la Recherche Agronomique, France for providing poplar clone INRA 717-1B4, Hongduyen Pham and Margot Chen for tissue culture assistance, Yingying Zhu for RNA from developmentally staged leaves and Liang-Jiao Xue for guidance on RNA-seq data processing. We additionally thank the Department of Energy Joint Genome Institute and collaborators for prepublication access to the *Populus tremula* x *P. alba* (IRNA 717-1B4) genome sequence and annotation.

SUPPORTING INFORMATION

Table S1. Primers used in this study.

Figure S1. PCR confirmation of NA alleles using allele-specific primers.

Figure S2. Sequence alignment of wild type and fusion *MYB* alleles from KO-5 and KO-69.

Dataset S1. CRISPR/Cas9 mutation patterns of the eight target *MYB* alleles in ΔG and KO lines.

Dataset S2. Assessment of off-target activity in trichomeless mutants.

FIGURE LEGENDS

Figure 1. Expression of clade 15 *MYB* transcription factors during *Populus* leaf maturation.
A simplified phylogenetic tree is shown with duplication history noted on the left. Data are mean±SD of n=3. LPI, leaf plastochron index; FPKM, fragments per kilobase of transcript per million mapped reads; MYB186, Potri.008G089200; MYB138, Potri.008G089700; MYB38, Potri.010G165700; and MYB83, Potri.017G086300.

Figure 2. CRISPR/Cas9 KO of trichome-regulating *MYBs*.
A, Schematic illustrations of the *MYB* gene structure, gRNA target site, and base pairing between the genomic target (black) and the gRNA spacer (red)-scaffold (blue) molecule. Black line denotes the protospacer adjacent motif (PAM). **B**, Zoomed-in view of the ΔG vector configuration at the gRNA spacer-scaffold junction with a guanine omission. **C-R**, Representative shoot tip (C, G, K, O) and LPI-1 abaxial (D, H, L, P) phenotypes and SEM images (E, F, I, J, M, N, Q, R) of soil-grown WT (D, E), Cas9 vector control (C), ΔG control (G-I), KO-27 (K-M), and null mutant (O-Q) plants, and leaf abaxial (F, N) or adaxial (J, R) images of tissue cultured ΔG (F, J) and null mutant (N, R) plants. Scale bar = 3 mm (D, H, L, P), 500 μm (E, I, M), 1 mm (Q), or 25 μm (F, J, N, R).

Figure 3. Mutation analysis of trichomeless mutants.

480 **A**, Schematic illustration of *MYB186* and *MYB138* on Chr8 subgenomes (main and alternative, or Chr8m
481 and Chr8a, respectively) and *MYB38* on Chr10m and Chr10a of the 717 genome. Neighboring genes are
482 color coded for synteny and the putative duplication block containing *MYB186* and *MYB138* on Chr8 is
483 marked by red brackets. Black triangles denote the eight gRNA target sites. **B**, Mutation spectrum
484 determined by amplicon sequencing. The eight alleles are arranged by genomic position for each plant
485 line and color-coded for the editing outcomes: green, unedited; orange, indel; and grey, no amplification
486 (NA). **C**, Representative amplicon sequencing output of three mutant events. All eight alleles, their
487 detection frequencies and indel patterns (mapped read count and percentage with the indicated
488 pattern) are shown and colored as in B. The gRNA target sequence is shown on top and protospacer
489 adjacent motif underlined. Allele-discriminating SNPs are shown in pink (see Supplemental Dataset S1
490 for the full data). **D**, Pie chart summary of the overall (left) and indel (right) editing patterns.
491
492 **Figure 4.** PCR analysis of selected mutant lines.
493 **A**, PCR amplification of the six *MYB* alleles on Chr8 from two WT, one ΔG and four KO lines. The four KO
494 lines were selected to represent one (KO-5 and KO-69) or two (KO-63 and KO-70) remaining Chr08
495 alleles. *UBC* (ubiquitin-conjugating enzyme) was included as loading control. M, molecular weight
496 marker; ntc, no-template control. **B**, Mutation patterns of Chr08 alleles in the selected mutant lines as
497 shown in Figure 3B. Orange triangles connected by dashes represent fusion junctions shown in C. **C**,
498 Sanger sequencing of PCR products from A. Sequence alignment of the six alleles flanking the gRNA
499 target site (red) is shown on top and chromatograms of the same region are shown below. Grey shaded
500 alignments are introns, with allele-discriminating SNPs shown in pink and homologous intron 2
501 sequences in blue (shifted upstream by 21 bp in *138m1* and *186m2* due to gaps). PAM is underlined and
502 boxed in blue for correspondence with the sequence traces below. Black triangles denote the Cas9
503 cleavage site and black dashed box corresponds to the 2-bp deletion (-2) detected in KO-5 and KO-69.
504 The two fusion alleles as determined by SNPs are marked below the KO-5 and KO-69 traces (see
505 Supplemental Figure S2 for the full sequence alignment).
506
507 **Figure 5.** Cuticular wax composition of trichomeless and control leaves.
508 **A**, Total wax load. **B**, Major classes of cuticular wax. **C**, Fatty alcohols (C26, 1-hexacosanol; C28, 1-
509 octacosanol) in wax (left) or whole leaves (right). **D**, β-sitosterol detected in wax (left) or whole leaves
510 (right). **E**, Triterpenes detected in wax (top) or whole leaves (bottom). Ergosterone, 14,24-dimethyl-
511 ergosta-8,25-dien-3-one; cycloartanone, 24-methylene cycloartan-3-one; lanosterone, lanosta-8,24-

512 dien-3-one. Data are mean±SD of n=5. All concentration estimates were based on sorbitol equivalent.
513 Statistical significance was determined by 2-tailed *t*-test (* $P<0.05$, ** $P<0.01$, *** $P<0.001$). nd, not
514 detected.
515
516
517 **REFERENCES**

518 **Armario Najera V, Twyman RM, Christou P, Zhu C** (2019) Applications of multiplex genome editing in
519 higher plants. Current Opinion in Biotechnology **59:** 93-102
520 **Bewg WP, Ci D, Tsai C-J** (2018) Genome editing in trees: From multiple repair pathways to long-term
521 stability. Frontiers in Plant Science **9:** 1732
522 **Braatz J, Harloff H-J, Mascher M, Stein N, Himmelbach A, Jung C** (2017) CRISPR-Cas9 targeted
523 mutagenesis leads to simultaneous modification of different homoeologous gene copies in
524 polyploid oilseed rape (*Brassica napus*). Plant Physiology **174:** 935-942
525 **Catchen JM, Amores A, Hohenlohe P, Cresko W, Postlethwait JH** (2011) Stacks: Building and genotyping
526 loci *de novo* from short-read sequences. Genes Genomes Genetics **1:** 171-182
527 **Čermák T, Curtin SJ, Gil-Humanes J, Čegan R, Kono TJY, Konečná E, Belanto JJ, Starker CG, Mathre JW,**
528 **Greenstein RL, Voytas DF** (2017) A multipurpose toolkit to enable advanced genome
529 engineering in plants. Plant Cell **29:** 1196-1217
530 **Chen K, Wang Y, Zhang R, Zhang H, Gao C** (2019) CRISPR/Cas Genome Editing and Precision Plant
531 Breeding in Agriculture. Annual Review of Plant Biology **70:** 667-697
532 **Dellaporta SL, Wood J, Hicks JB** (1983) A plant DNA minipreparation: Version II. Plant Molecular Biology
533 Reporter **1:** 19-21
534 **Dmitruk M, Sulborska A, Żuraw B, Stawiarz E, Weryszko-Chmielewska E** (2019) Sites of secretion of
535 bioactive compounds in leaves of *Dracocephalum moldavica* L.: anatomical, histochemical, and
536 essential oil study. Brazilian Journal of Botany **42:** 701-715
537 **Dobin A, Gingeras TR** (2015) Mapping RNA-seq reads with STAR. Curr Protoc Bioinformatics **51:**
538 11.14.11-11.14.19
539 **Endo A, Masafumi M, Kaya H, Toki S** (2016) Efficient targeted mutagenesis of rice and tobacco genomes
540 using Cpf1 from Francisella novicida. Scientific Reports **6:** 38169
541 **Falginella L, Andre CM, Legay S, Lin-Wang K, Dare AP, Deng C, Rebstock R, Plunkett BJ, Guo L, Cipriani**
542 **G, Espley RV** (2021) Differential regulation of triterpene biosynthesis induced by an early failure
543 in cuticle formation in apple. Horticulture Research **8:** 75
544 **Flagel LE, Wendel JF** (2009) Gene duplication and evolutionary novelty in plants. New Phytol **183:** 557-
545 564
546 **Gao Y, Zhao Y** (2014) Self-processing of ribozyme-flanked RNAs into guide RNAs in vitro and in vivo for
547 CRISPR-mediated genome editing. Journal of Integrative Plant Biology **56:** 343-349
548 **Germini D, Tsfasman T, Zakharova VV, Sjakste N, Lipinski M, Vassetzky Y** (2018) A comparison of
549 techniques to evaluate the effectiveness of genome editing. Trends in Biotechnology **36:** 147-
550 159
551 **Hahn F, Eisenhut M, Mantegazza O, Weber APM** (2018) Homology-directed repair of a defective
552 *Glabrous* gene in *Arabidopsis* with Cas9-based gene targeting. Frontiers in Plant Science **9:** 424
553 **Hahn F, Mantegazza O, Greiner A, Hegemann P, Eisenhut M, Weber AP** (2017) An efficient visual screen
554 for CRISPR/Cas9 activity in *Arabidopsis thaliana*. Frontiers in Plant Science **8:** 39
555 **Hegebarth D, Buschhaus C, Wu M, Bird D, Jetter R** (2016) The composition of surface wax on trichomes
556 of Arabidopsis thaliana differs from wax on other epidermal cells. Plant Journal **88:** 762-774

557 **Holwerda EK, Thorne PG, Olson DG, Amador-Noguez D, Engle NL, Tschaplinski TJ, van Dijken JP, Lynd**
558 **LR** (2014) The exometabolome of *Clostridium thermocellum* reveals overflow metabolism at high
559 cellulose loading. Biotechnology for Biofuels **7:** 155
560 **Jacobs TB, LaFayette PR, Schmitz RJ, Parrott WA** (2015) Targeted genome modifications in soybean with
561 CRISPR/Cas9. BMC Biotechnology **15:** 16
562 **Jinek M, Chylinski K, Fonfara I, Hauer M, Doudna JA, Charpentier E** (2012) A Programmable dual-RNA-
563 guided DNA endonuclease in adaptive bacterial immunity. Science **337:** 816-821
564 **Koncz C, Schell J** (1986) The promoter of TL-DNA gene *5* controls the tissue-specific expression of
565 chimaeric genes carried by a novel type of *Agrobacterium* binary vector. Molecular & General
566 Genetics **204:** 383-396
567 **Lange BM, Turner GW** (2013) Terpenoid biosynthesis in trichomes--current status and future
568 opportunities. Plant Biotechnol J **11:** 2-22
569 **Li A, Jia S, Yobi A, Ge Z, Sato SJ, Zhang C, Angelovici R, Clemente TE, Holding DR** (2018) Editing of an
570 alpha-kafirin gene family increases, digestibility and protein quality in sorghum. Plant Physiology
571 **177:** 1425-1438
572 **Li J-F, Norville JE, Aach J, McCormack M, Zhang D, Bush J, Church GM, Sheen J** (2013) Multiplex and
573 homologous recombination–mediated genome editing in *Arabidopsis* and *Nicotiana*
574 *benthamiana* using guide RNA and Cas9. Nature Biotechnology **31:** 688-691
575 **Liao Y, Smyth GK, Shi W** (2014) featureCounts: an efficient general purpose program for assigning
576 sequence reads to genomic features. Bioinformatics **30:** 923-930
577 **Lowder LG, Zhang D, Baltes NJ, Paul JW, Tang X, Zheng X, Voytas DF, Hsieh T-F, Zhang Y, Qi Y** (2015) A
578 CRISPR/Cas9 toolbox for multiplexed plant genome editing and transcriptional regulation. Plant
579 Physiology **169:** 971-985
580 **Ma X, Zhang Q, Zhu Q, Liu W, Chen Y, Qiu R, Wang B, Yang Z, Li H, Lin Y, Xie Y, Shen R, Chen S, Wang Z,**
581 **Chen Y, Guo J, Chen L, Zhao X, Dong Z, Liu Y-G** (2015) A robust CRISPR/Cas9 system for
582 convenient, high-efficiency multiplex genome editing in monocot and dicot plants. Molecular
583 Plant **8:** 1274-1284
584 **McCarty NS, Graham AE, Studená L, Ledesma-Amaro R** (2020) Multiplexed CRISPR technologies for
585 gene editing and transcriptional regulation. Nature Communications **11:** 1281
586 **Meilan R, Ma C** (2006) Poplar (*Populus* spp.). *In* K Wang, ed, Agrobacterium Protocols Volume 2.
587 Methods in Molecular Biology, Vol 344. Humana Press, Totowa, NJ
588 **Mikami M, Toki S, Endo M** (2017) In planta processing of the SpCas9–gRNA complex. Plant and Cell
589 Physiology **58:** 1857-1867
590 **Nasti RA, Voytas DF** (2021) Attaining the promise of plant gene editing at scale. Proceedings of the
591 National Academy of Sciences **118:** e2004846117
592 **Nekrasov V, Staskawicz B, Weigel D, Jones JDG, Kamoun S** (2013) Targeted mutagenesis in the model
593 plant Nicotiana benthamiana using Cas9 RNA-guided endonuclease. Nature Biotechnology **31:**
594 691-693
595 **Norris SR, Barrette TR, DellaPenna D** (1995) Genetic dissection of carotenoid synthesis in Arabidopsis
596 defines plastoquinone as an essential component of phytoene desaturation. Plant Cell **7:** 2139-
597 2149
598 **Panchy N, Lehti-Shiu M, Shiu S-H** (2016) Evolution of gene duplication in plants. Plant Physiology **171:**
599 2294-2316
600 **Plett JM, Wilkins O, Campbell MM, Ralph SG, Regan S** (2010) Endogenous overexpression of *Populus*
601 *MYB186* increases trichome density, improves insect pest resistance, and impacts plant growth.
602 Plant Journal **64:** 419-432
603 **Qi L, Haurwitz RE, Shao W, Doudna JA, Arkin AP** (2012) RNA processing enables predictable
604 programming of gene expression. Nature Biotechnology **30:** 1002-1006

605 **Santos Tozin LRd, de Melo Silva SC, Rodrigues TM** (2016) Non-glandular trichomes in Lamiaceae and
606 Verbenaceae species: morphological and histochemical features indicate more than physical
607 protection. New Zealand Journal of Botany **54:** 446-457
608 **Shan Q, Wang Y, Li J, Zhang Y, Chen K, Liang Z, Zhang K, Liu J, Xi JJ, Qiu J-L, Gao C** (2013) Targeted
609 genome modification of crop plants using a CRISPR-Cas system. Nat Biotech **31:** 686-688
610 **Stemmer M, Thumberger T, del Sol Keyer M, Wittbrodt J, Mateo JL** (2015) CCTop: An intuitive, flexible
611 and reliable CRISPR/Cas9 target prediction tool. PLoS ONE **10:** e0124633
612 **Tang X, Ren Q, Yang L, Bao Y, Zhong Z, He Y, Liu S, Qi C, Liu B, Wang Y, Sretenovic S, Zhang Y, Zheng X,**
613 **Zhang T, Qi Y, Zhang Y** (2019) Single transcript unit CRISPR 2.0 systems for robust Cas9 and
614 Cas12a mediated plant genome editing. Plant Biotechnology Journal **17:** 1431-1445
615 **Tang X, Zheng X, Qi Y, Zhang D, Cheng Y, Tang A, Voytas Daniel F, Zhang Y** (2016) A single transcript
616 CRISPR-Cas9 system for efficient genome editing in plants. Molecular Plant **9:** 1088-1091
617 **Tsai C-J, Xu P, Xue L-J, Hu H, Nyamdari B, Naran R, Zhou X, Goeminne G, Gao R, Gjersing E, Dahlen J,**
618 **Pattathil S, Hahn MG, Davis M, Ralph J, Boerjan WA, Harding SA** (2020) Compensatory guaiacyl
619 lignin biosynthesis at the expense of syringyl lignin in *4CL1*-knockout poplar. Plant Physiology
620 **183:** 123-136
621 **Wang B, Luo Q, Li Y, Yin L, Zhou N, Li X, Gan J, Dong A** (2020) Structural insights into target DNA
622 recognition by R2R3-MYB transcription factors. Nucleic Acids Research **48:** 460-471
623 **Wang M, Mao Y, Lu Y, Wang Z, Tao X, Zhu J-K** (2018) Multiplex gene editing in rice with simplified
624 CRISPR-Cpf1 and CRISPR-Cas9 systems. Journal of Integrative Plant Biology **60:** 626-631
625 **Wilkins O, Nahal H, Foong J, Provart NJ, Campbell MM** (2009) Expansion and diversification of the
626 *Populus* R2R3-MYB family of transcription factors. Plant Physiology **149:** 981-993
627 **Xie K, Minkenberg B, Yang Y** (2015) Boosting CRISPR/Cas9 multiplex editing capability with the
628 endogenous tRNA-processing system. Proceedings of the National Academy of Sciences **112:**
629 3570-3575
630 **Xing H-L, Dong L, Wang Z-P, Zhang H-Y, Han C-Y, Liu B, Wang X-C, Chen Q-J** (2014) A CRISPR/Cas9
631 toolkit for multiplex genome editing in plants. BMC Plant Biology **14:** 327
632 **Xue L-J, Alabady MS, Mohebbi M, Tsai C-J** (2015) Exploiting genome variation to improve next-
633 generation sequencing data analysis and genome editing efficiency in Populus tremula x alba
634 717-1B4. Tree Genetics & Genomes **11:** 82
635 **Xue LJ, Tsai CJ** (2015) AGEseq: Analysis of genome editing by sequencing. Molecular Plant **8:** 1428-1430
636 **Yang L, Güell M, Niu D, George H, Lesha E, Grishin D, Aach J, Shrock E, Xu W, Poci J, Cortazio R,**
637 **Wilkinson RA, Fishman JA, Church G** (2015) Genome-wide inactivation of porcine endogenous
638 retroviruses (PERVs). Science **350:** 1101-1104
639 **Zhang Y, Bai Y, Wu G, Zou S, Chen Y, Gao C, Tang D** (2017) Simultaneous modification of three
640 homoeologs of TaEDR1 by genome editing enhances powdery mildew resistance in wheat. Plant
641 Journal **91:** 714-724
642 **Zhou X, Jacobs TB, Xue L-J, Harding SA, Tsai C-J** (2015) Exploiting SNPs for biallelic CRISPR mutations in
643 the outcrossing woody perennial *Populus* reveals 4-coumarate:CoA ligase specificity and
644 redundancy. New Phytologist **208:** 298-301
645 **Zwaenepoel A, Van de Peer Y** (2018) wgd—simple command line tools for the analysis of ancient whole-
646 genome duplications. Bioinformatics **35:** 2153-2155

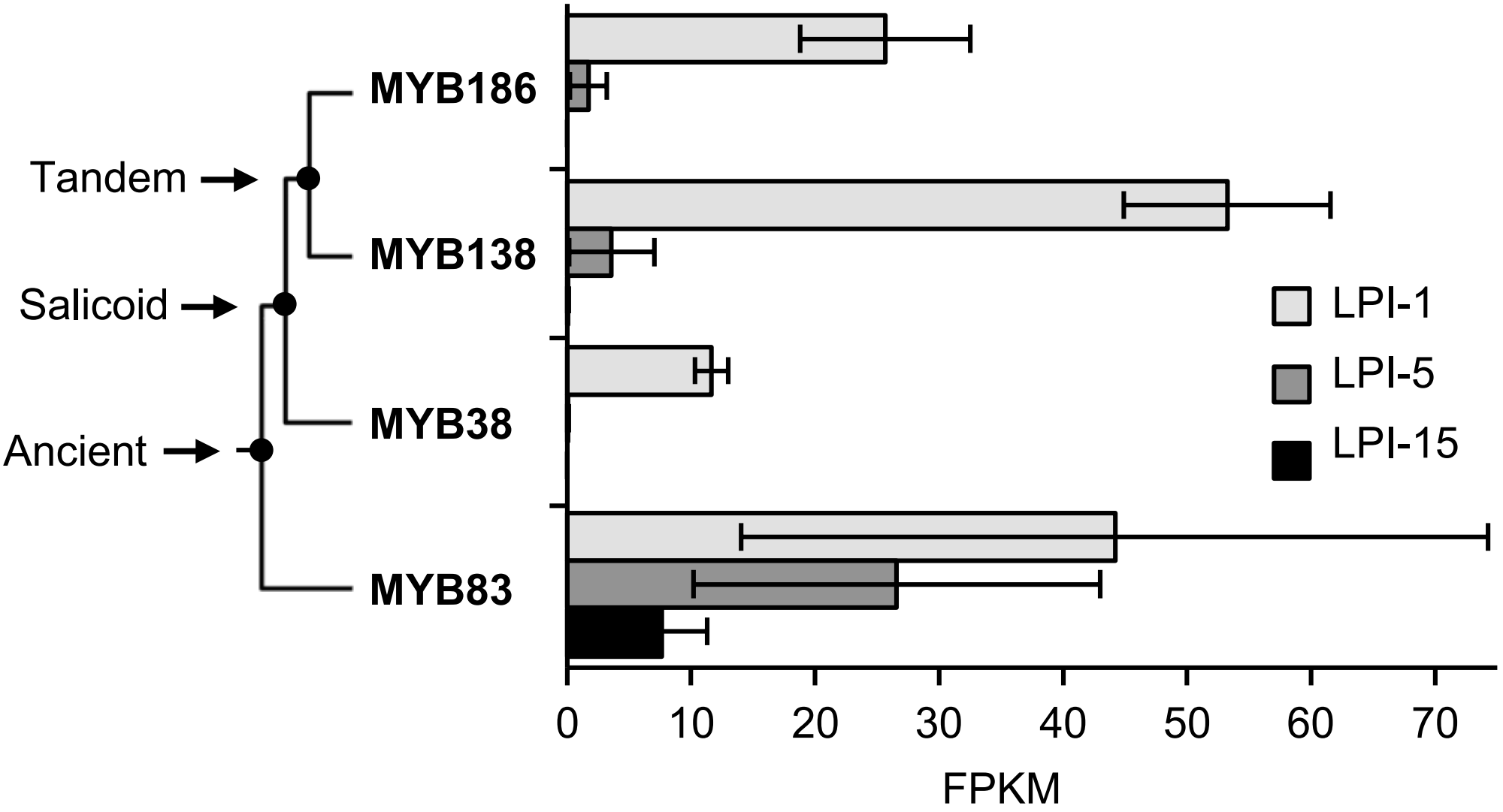

Figure 1. Expression of clade 15 *MYB* transcription factors during *Populus* leaf maturation. A simplified phylogenetic tree is shown with duplication history noted on the left. Data are mean ± SD of n=3. LPI, leaf plastochron index; FPKM, fragments per kilobase of transcript per million mapped reads; MYB186, Potri.008G089200; MYB138, Potri.008G089700; MYB38, Potri.010G165700; and MYB83, Potri.017G086300.

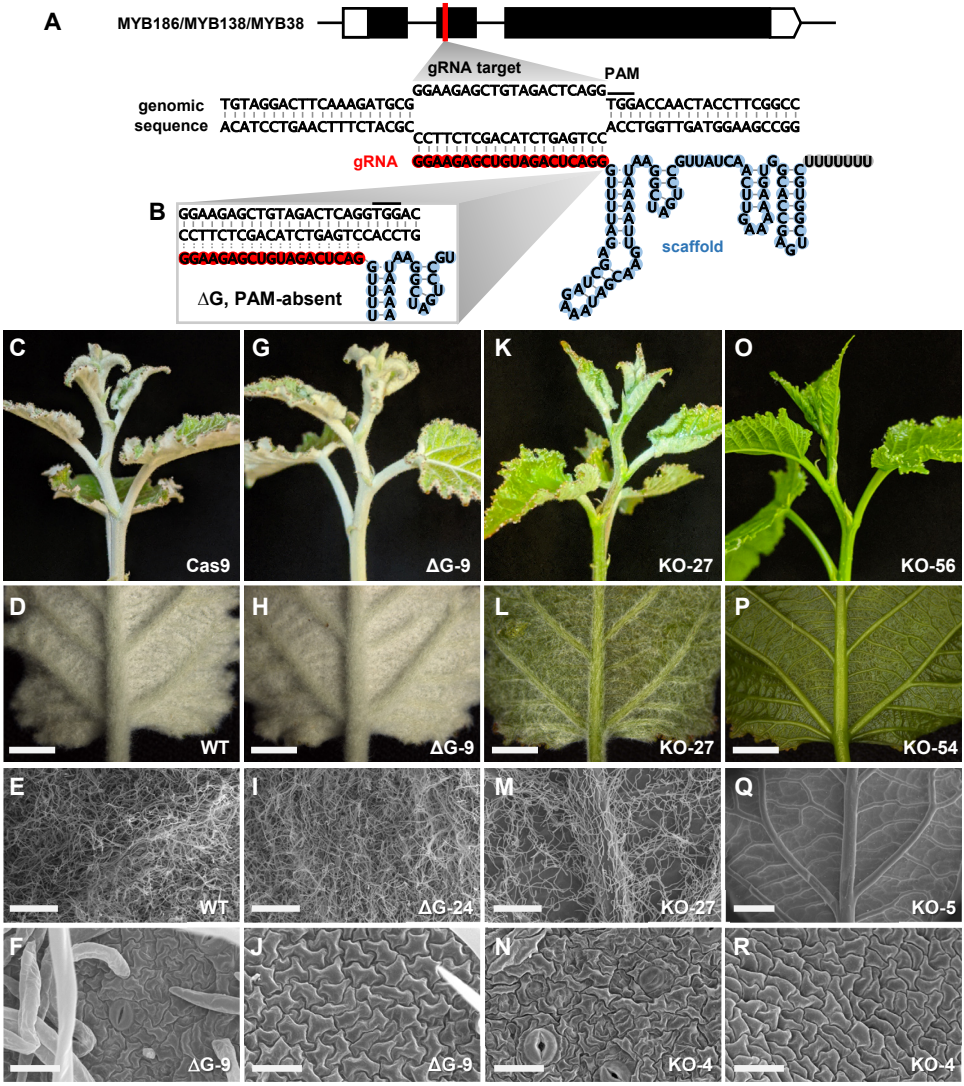

Figure 2. CRISPR/Cas9 KO of trichome-regulating *MYBs*. **A**, Schematic illustrations of the *MYB* gene structure, gRNA target site, and base pairing between the genomic target (black) and the gRNAspacer (red)-scaffold (blue) molecule. Black line denotes the protospacer adjacent motif (PAM). **B**, Zoomed-in view of the ΔG vector configuration at the gRNA spacer-scaffold junction with a guanine omission. **C-R**, Representative shoot tip (C, G, K, O) and LPI-1 abaxial (D, H, L, P) phenotypes and SEM images (E, F, I, J, M, N, Q, R) of soil-grown WT (D, E), Cas9 vector control (C), ΔG control (G-I), KO-27 (K-M), and mutant (O-Q) plants, and leaf abaxial (F, N) or adaxial (J, R) images of tissue cultured ΔG (F, J) and mutant (N, R) plants. Scale bar = 3 mm (D, H, L, P), 500 μm (E, I, M), 1 mm (Q), or 25 μm (F, J, N, R).

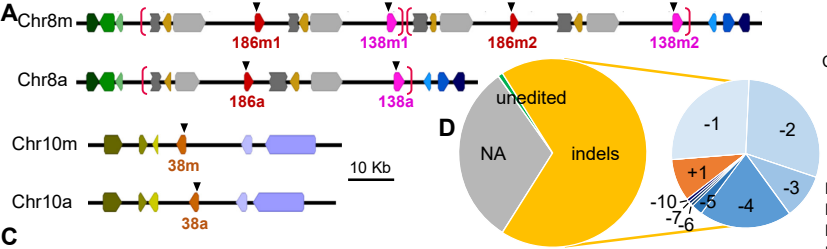

B

	Main Chr8				Alt. Chr8		Chr10	
	186m1	138m1	186m2	138m2	186a	138a	38m	38a
Control								
ΔG								
KO-2	+1	-2			-1		-2	-1
KO-4	-1			-4	-2	-1	-2	+1
KO-5	-2						-4	-1
KO-7	-1	-2			-1	-4	-1	-3
KO-10		-1		-1			-3	-4
KO-12	-1		-1		-10	-3	-7	-2
KO-18		+1			-2		-1	-2
KO-19	-1	-4	-2	-4	-1	-2	-4	-2
KO-22					-2	-1	-2	-4
KO-24				-1	-3	-3	-1	-2
KO-25	-4	-2	-4	-1	-4	-2	-1	-4
KO-26		-3	-3		-4	+1		-2
KO-27	-2	+1	-2	-1	-2	-3		
KO-28	-4	-2	-1	-4	+1	-2	+1	-1
KO-29	+1	-2		-2	-2		-1	-2
KO-30			-2	-6	-4	-4	-1	
KO-33			-2	-4	-1	-3	-2	-1
KO-39	-2	-1			-2	-1	-1	-1
KO-40	-5			-3	+1	+1	-1	-4
KO-44		-1		+1			-1	-1
KO-46	-2	-2	-2	-1	-2	-2	-2	-3
KO-48	-4	-2		-1			-1	-2
KO-54	-1		-1		-2	-3	+1	-4
KO-56			-1	-5	+1	-1		+1
KO-61				-4	-3		-3	-2
KO-62	-4	-4	-4	-1	-2	+1	-2	-2
KO-63					-4	-2		-4
KO-67			-5	-4	-1	-4	-2	-4
KO-69		-2					-5	-3
KO-70	-4				-3		-4	-4

Unedited indel NA (no amplification)

C

Line	Allele	Read sequence	gRNA: GGAAGAGCTGTAGACTC.AGGTGG	Read #	%	Indel
KO-19	186m1	TGCGTGCGTGTGTGTAGGACTTCAAAGATGCGGGAAGAGCTGTAGACT-.AGGTGGACC		212	99.1	-1
	138m1	GGTGCGTGCGTGTATAGGACTTCAAAGATGCGGGAAGAGCTGTAG----.AGGTGGACC		233	99.1	-4
	186m2	TGTGTGCGTGTGTGTAGGACTTCAAAGATGCGGGAAGAGCTGTAGAC--.AGGTGGACC		198	98.0	-2
	138m2	CGTGTGTGTGTGTATAGGACTTCAAAGATGCGGGAAGAGCTGTAG----.AGGTGGACC		176	98.9	-4
	186a	TGTGTGTGTGTGTGTAGGACTTCAGAGATGCGGGAAGAGCTGTAGACT-.AGGTGGACC		185	99.5	-1
	138a	TGTGTGTGTGTGTGTAGGACTTCAGAGATGCGGGAAGAGCTGTAGAC--.AGGTGGACC		219	97.7	-2
	38m	GGTCTACATATATACAGGGCTTCAAAGATGTGGGAAGAGCTGTAG----.AGGTGGACT		319	96.9	-4
	38a	GGTCTACATATATACAGGGCTTCAAAGATGCGGGAAGAGCTGTAGAC--.AGGTGGACT		308	98.7	-2
KO-27	186m1	TGCGTGCGTGTGTGTAGGACTTCAAAGATGCGGGAAGAGCTGTAG--TC.AGGTGGACC		252	100	-2
	138m1	GGTGCGTGCGTGTATAGGACTTCAAAGATGCGGGAAGAGCTGTAGACTCAAGGTGGACC		211	99.1	+1
	186m2	TGTGTGCGTGTGTGTAGGACTTCAAAGATGCGGGAAGAGCTGTAGACTC.--GTGGACC		144	96.6	-2
	138m2	CGTGTGTGTGTGTATAGGACTTCAAAGATGCGGGAAGAGCTGTAGACT-.AGGTGGACC		273	98.9	-1
	186a	TGTGTGTGTGTGTGTAGGACTTCAGAGATGCGGGAAGAGCTGTAGAC--.AGGTGGACC		228	100	-2
	138a	TGTGTGTGTGTGTGTAGGACTTCAGAGATGCGGGAAGAGCTGTAGA---.AGGTGGACC		220	99.1	-3
	38m	GGTCTACATATATACAGGGCTTCAAAGATGTGGGAAGAGCTGTAGACTC.AGGTGGACT		358	92.0	WT
	38a	GGTCTACATATATACAGGGCTTCAAAGATGCGGGAAGAGCTGTAGACTC.AGGTGGACT		312	93.1	WT
KO-69	186m1			3	-	NA
	138m1	GGTGCGTGCGTGTATAGGACTTCAAAGATGCGGGAAGAGCTGTAGAC--.AGGTGGACC		544	99.8	-2
	186m2			4	-	NA
	138m2			7	-	NA
	186a			0	-	NA
	138a			1	-	NA
	38m	GGTCTACATATATACAGGGCTTCAAAGATGTGGGAAGAGCTGTAGA---.--GTGGACT		707	99.2	-5
	38a	GGTCTACATATATACAGGGCTTCAAAGATGCGGGAAGAGCTGTAGA---.AGGTGGACT		629	99.4	-3

Figure 3. Mutation analysis of trichomeless mutants. **A**, Schematic illustration of *MYB186* and *MYB138* on Chr8 subgenomes (main and alternative, or Chr8m and Chr8a, respectively) and *MYB38* on Chr10m and Chr10a of the 717 genome. Neighboring genes are color coded for synteny and the putative duplication block containing *MYB186* and *MYB138* on Chr8 is marked by red brackets. Black triangles denote the eight gRNA target sites. **B**, Mutation spectrum determined by amplicon sequencing. The eight alleles are arranged by genomic position for each plant line and color-coded for the editing outcomes: green, unedited; orange, indel; and grey, no amplification (NA). **C**, Representative amplicon sequencing output of three mutant events. All eight alleles, their detection frequencies and the indel patterns (mapped read count and percentage with the indicated pattern) are shown and colored as in B. The gRNA target sequence is shown on top and protospacer adjacent motif underlined. Allele-discriminating SNPs are shown in pink (see Supplemental Dataset S1 for the full data). **D**, Pie chart summary of the overall (left) and indel (right) editing patterns.

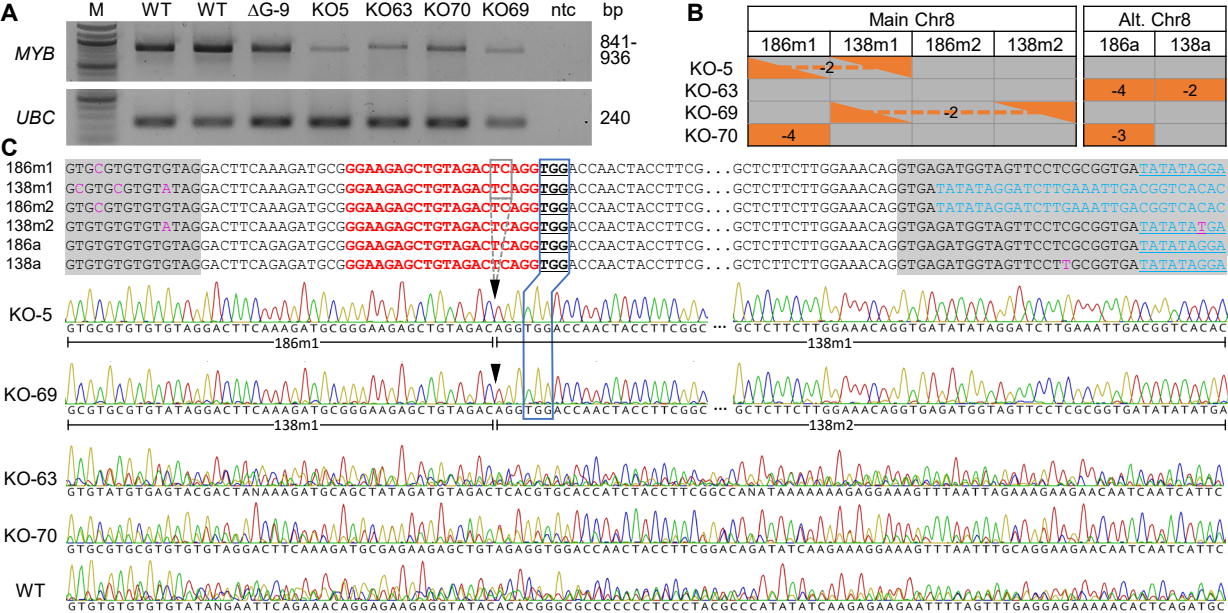

Figure 4. PCR analysis of selected mutant lines. **A**, PCR amplification of the six *MYB* alleles on Chr8 from two WT, one ΔG and four KO lines. The four KO lines were selected to represent one (KO-5 and KO-69) or two (KO-63 and KO-70) remaining Chr08 alleles. *UBC* (ubiquitin-conjugating enzyme) was included as loading control. M, molecular weight marker; ntc, no-template control. **B**, Mutation patterns of Chr08 alleles in the selected mutant lines as shown in Figure 3B. Orange triangles connected by dashes represent fusion junctions shown in C. **C**, Sanger sequencing of PCR products from A. Sequence alignment of the six alleles flanking the gRNA target site (red) is shown on top and chromatograms of the same region are shown below. Grey shaded alignments are introns, with allele-discriminating SNPs shown in pink and homologous intron 2 sequences in blue (shifted upstream by 21 bp in *138m1* and *186m2* due to gaps). PAM is underlined and boxed in blue for correspondence with the sequence traces below. Black triangles denote the Cas9 cleavage site and black dashed box corresponds to the 2-bp deletion (-2) detected in KO-5 and KO-69. The two fusion alleles as determined by SNPs are marked below the KO-5 and KO-69 traces (see Supplemental Figure S2 for the full sequence alignment).

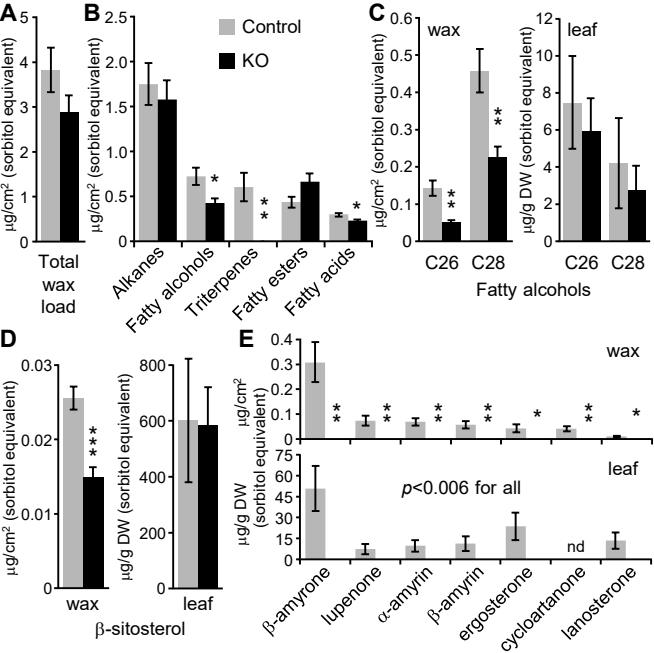

Figure 5. Cuticular wax composition of trichomeless and control leaves. **A**, Total wax load. **B**, Major classes of cuticle wax. **C**, Fatty alcohols (C26, 1-hexacosanol; C28, 1-octacosanol) detected in wax (left) or whole leaves (right). **D**, β-sitosterol detected in wax (left) or whole leaves (right). **E**, Triterpenes detected in wax (top) or whole leaves (bottom). Ergosterone, 14,24-dimethyl-ergosta-8,25-dien-3-one; cycloartanone, 24-methylene cycloartan-3-one; lanosterone, lanosta-8,24-dien-3-one. Data are mean±SD of n=5. All concentration estimates were based on sorbitol equivalent. Statistical significance was determined by 2-tailed *t*-test (* $P<0.05$, ** $P<0.01$, *** $P<0.001$). nd, not detected.